Chemistry–A European Journal
Research Article
doi.org/10.1002/chem.202302476
Chemistry Europe
European Chemical Societies Publishing
www.chemeurj.org

Special Collection

# A Prato Tour on Carbon Nanotubes: Raman Insights

María Isabel Lucío,[a, b, c] Francesco Giacalone,[d] Valeria La Parola,[e] Sergio Gámez-Valenzuela,[f] Fernando Muñoz-Alba,[f] M. Carmen Ruiz Delgado,[f] M. Antonia Herrero,*[a, b] and Ester Vázquez*[a, b]

*Dedicated to Professor Maurizio Prato on the occasion of his retirement*

The functionalisation of carbon nanotubes has been instrumental in broadening its application field, allowing especially its use in biological studies. Although numerous covalent and non-covalent functionalisation methods have been described, the characterisation of the final materials has always been an added challenge. Among the various techniques available, Raman spectroscopy is one of the most widely used to determine the covalent functionalisation of these species. However, Raman spectroscopy is not a quantitative technique, and no studies are reported comparing its performance when the same number of functional groups are added but using completely different reactions. In this work, we have experimentally and theoretically studied the functionalisation of carbon nanotubes using two of the most commonly used reactions: 1,3-dipolar cycloaddition of azomethylene ylides and diazonium-based radical addition. The number of groups introduced onto the tubes by these reactions has been determined by different characterisation techniques. The results of this study support the idea that data obtained by Raman spectra are only helpful for comparing functionalisations produced using the same type of reaction. However, they should be carefully analysed when comparing functionalisations produced using different reaction types.

## Introduction

Since their discovery by Sumio Iijima in 1991, carbon nanotubes (CNT) have led to a breakthrough in materials chemistry, placing carbon nanomaterials at the centre of nanotechnology development.[1] Their extraordinary properties have led to a wide range of applications in fields as diverse as gene and drug delivery[2] and bioimaging,[3] catalysis,[4] reinforcement of materials,[5] photovoltaics[6] or sensing[7] and biosensing.[8] However, pristine CNTs tend to aggregate (Figure S1, Supporting Information) and are very insoluble in common solvents, therefore their chemical functionalisation is considered a key step to obtain materials useful in real-world applications.[9] Indeed, this process is critical for their use in biomedical applications as both improves their pharmacokinetics and diminishes their toxicity.[10]

Several reactions have been developed to modify CNTs by covalent[11–15] and non-covalent functionalisation.[16] Non-covalent modification usually takes place between the sidewall of the tubes and surfactants, polymers or aromatic compounds via hydrophobic interactions or π–π stacking, with the hybrids obtained maintaining their electronic properties. Covalent functionalisation introduces molecular entities on CNTs by way of a direct sidewall functionalisation in which the attack on the $sp^2$ structure produces a rehybridization of the carbon atoms into a $sp^3$ configuration. This modification directly alters the

[a] M. Isabel Lucío, M. A. Herrero, E. Vázquez
Departamento de Química Inorgánica, Orgánica y Bioquímica, Facultad de Ciencias y Tecnologías Químicas-IRICA
Universidad de Castilla-La Mancha
13071 Ciudad Real (Spain)
E-mail: mariaantonia.herrero@uclm.es
ester.vazquez@uclm.es

[b] M. Isabel Lucío, M. A. Herrero, E. Vázquez
Instituto Regional de Investigación Científica Aplicada (IRICA)
Universidad de Castilla-La Mancha
13071 Ciudad Real (Spain)

[c] M. Isabel Lucío
Current affiliation:
Instituto Interuniversitario de Investigación de Reconocimiento Molecular y Desarrollo Tecnológico (IDM)
Universitat Politécnica de Valéncia, Universitat de Valéncia
Camino de Vera s/n, 46022 Valencia (Spain)

[d] F. Giacalone
Department of Biological, Chemical and Pharmaceutical Sciences and Technologies (STEBICEF)
University of Palermo and INSTM UdR – Palermo
Viale delle Scienze, Ed.17, 90128 Palermo (Italy)

[e] V. La Parola
Istituto per lo Studio dei Materiali Nanostrutturati ISMN-CNR
Via Ugo La Malfa 153, 90146 Palermo (Italy)

[f] S. Gámez-Valenzuela, F. Muñoz-Alba, M. C. Ruiz Delgado
Department of Physical Chemistry
University of Malaga
Campus de Teatinos s/n, 29071 Malaga (Spain)

Supporting information for this article is available on the WWW under https://doi.org/10.1002/chem.202302476

Special Collection This article is part of a joint Special Collection in honor of Maurizio Prato.

unique electronic properties of the CNTs, which may be detrimental to some potential applications. Nonetheless, covalent functionalisation is still preferred in many cases as it yields more stable materials.[11] Indeed, it is especially valuable when the attachment of the desired functionality onto the carbon nanostructure requires sequential or orthogonal chemical reactions.[17]

The 1,3-dipolar cycloaddition of azomethine ylides and the diazonium-based radical addition described by Prato[18] and Tour,[19] respectively, are among the most widely used chemical reactions to covalently modify CNTs. For example, since the first report[10] on the mitigation of the pathogenicity of CNTs after their functionalisation using the so-called Prato reaction,[20–22] countless studies have used it to study the biomedical applications of CNTs.[23,24] The Tour approach has also proved very useful for multiple applications.[25] In addition, the combination of both reactions can be used to introduce orthogonal functional groups,[26] even in other carbon nanostructures.[27]

As covalent approaches, both reactions alter the $sp^2$ configuration of the carbon atoms to $sp^3$. Rehybridization is usually monitored by Raman spectroscopy as an increase in the D band of CNTs at 1314 $cm^{-1}$.[28,29] However, some authors have recently shown that covalent functionalisation can be performed on the nanotube walls without altering the D band, and thus without altering their π-conjugated electronic structure.[30] Although the no modification of the D could be associated to a low level of functionalization, these findings suggest that, in this case, the functionalization is high but the reaction is carried out in one step via a mechanism that includes ring-opening and rehybridization stages. On the other hand, although it is well established that D-band enhancement in carbon nanomaterials is related to increased functionalisation using reactions such as diazonium-based radical addition,[31] Raman spectroscopy is not a quantitative technique. Moreover, there are no available studies comparing D-band growth when the same number of functional groups are added but using completely different reactions.

In this work, we have modified CNTs using both the Prato and Tour approaches to study whether the immobilization of organic moieties on the sidewalls of the tubes alters the density of defects present in the materials. The resulting functionalised CNTs were characterised by thermogravimetric analysis (TGA) and Raman spectroscopy. Additionally, X-ray photoelectron spectroscopy (XPS) enabled semi-quantification of the number of groups introduced during organic functionalisation by analysing the heteroatoms, *i.e.*, nitrogen, bromine and chlorine, introduced during the reactions. Finally, theoretical calculations were performed to study how the introduction of functional groups in each type of reaction influences the Raman spectra of the functionalised CNTs.

## Results and Discussion

### Experiments

This work focuses on monitoring the sidewall perturbation of carbon nanomaterials after covalent functionalisation using two particular chemical reactions. Single-walled carbon nanotubes (**SWCNTs**) were chosen as model nanostructures as they present a low density of $sp^3$ carbon atoms and, therefore, their modification can be easily monitored by Raman spectroscopy. Additionally, chemical moieties that include halogen elements were chosen for the functionalisation as the presence of these heteroatoms in the sample can be estimated by X-ray photoelectron spectroscopy (XPS). Thus, pristine single-walled carbon nanotubes (***p*-SWCNTs**) were functionalised by 1,3-dipolar cycloaddition of azomethine ylides using 4-chlorobenzaldehyde and sarcosine and following a protocol previously described by our group, using microwave irradiation under solvent-free conditions, to yield **SWCNTs-1** (Scheme 1).[26] Similarly, ***p*-SWCNTs** were functionalised by radical addition of 4-chloroaniline using isoamyl nitrite as oxidizing agent under microwave irradiation to yield **SWCNTs-2**. The reaction products were characterised using different spectroscopic and analytical techniques.

Figure 1 shows the thermogravimetric analysis of samples **SWCNTs-1** and **SWCNTs-2**. The weight loss at 700 °C can be associated with the quantity of functional groups attached to the walls of the carbon nanostructure because all the organic groups are decomposed at that temperature, while the SWCNTs themselves remain stable. As can be observed, both kinds of reactions introduce a similar quantity of organic material (19.5% and 17.9%). Taking into account the molecular weight of the groups introduced it is possible to calculate one functional group for every 57 carbon atoms in the **SWCNTs-1** derivatives, and one functional group for every 41 carbon atoms in the **SWCNTs-2** derivatives (Table 1). Another important feature observed in TGA is that **SWCNTs-1** are stable up to 300 °C, while **SWCNTs-2** start to lose weight below 200 °C.

Although TGA analysis gives information about the quantity of organic material immobilized on the carbon nanomaterial wall, it does not indicate the chemical composition of the attached moieties or whether the material is covalently or non-

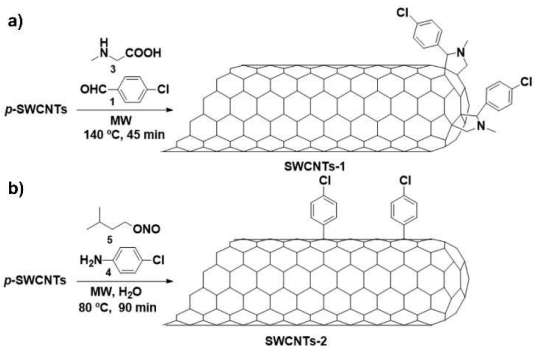


**Scheme 1.** a) Prato reaction of 4-chlorobenzaldehyde and sarcosine and ***p*-SWCNTs** using microwave activation. b) Diazonium-based radical addition of ***p*-SWCNTs** using 4-chloroaniline, isoamyl nitrite and microwave activation.

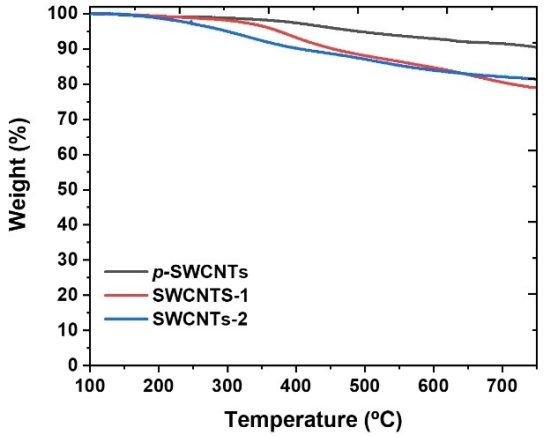


**Figure 1.** Thermogravimetric analysis of ***p*-SWCNTs**, **SWCNTs-1** and **SWCNTs-2**.

**Table 1.** Details of the TGA, Raman and XPS analysis of **SWCNTs-1** and **SWCNTs-2**.

| Sample | TGA | | Raman | XPS[d] | |
|---|---|---|---|---|---|
| | weight loss (%)[a] | C/FG[b] | $I_D/I_G$[c] | C/Cl | C/N |
| **SWCNTs-1** | 19.5 | 57 | 0.10 | 50 | 50 |
| **SWCNTs-2** | 17.9 | 41 | 0.43 | 50 | — |

[a] Weight loss was measured by TGA at 700 °C, [b] Number of carbons per functional group = $[(100-\%_{weightloss})\times MW_{functionalgroup}]/12\times\%_{weightloss}$. In this value, only the carbon atoms from the SWCNT walls, and not the one introduced with the functional group are considered. See Section 2 in the Supporting Information for more information. [c] $I_D/I_G$ is the relative integrated area of the D band (*i.e.*, ranging from 1200 to 1400 $cm^{-1}$) and the G band (*i.e.*, ranging from 1400 to 1830 $cm^{-1}$) in the Raman spectra. [d] Carbon refers to the total number of carbon atoms in the sample, *i.e.*, those from the SWCNT walls and those introduced with the functional group.

covalently attached. To shed light on this matter, X-ray photoelectron spectroscopy (XPS) and Raman spectroscopy were also performed. XPS is a semi-quantitative technique that provides information about the chemical composition of material surfaces as well as about the electronic state of elements and, therefore, the type of bonds present in a sample.[32] It is a generally accepted technique for the characterization of carbon nanomaterials and for the assessment of their functionalisation with heteroatoms, which is especially relevant for this study. As such, **SWCNTs-1** and **SWCNTs-2** were also characterised by XPS (Figure S2, supporting information). Table 1 shows the C/Cl and C/N ratios for every sample. It should be noticed that XPS values refer to the total carbon atom content and not only to the carbon atoms from the nanotube walls. As can be observed, **SWCNTs-2** derivatives did not show nitrogen atoms in their composition, while the hybrid **SWCNTs-1** exhibited nitrogen introduced through the sarcosine amino acid. As expected, both samples present chlorine atoms. The number of Cl atoms is consistent with the N atoms in **SWCNTs-1**. C/Cl values can be directly related to the number of functional groups per carbon atom as every functional group has one chlorine atom. Therefore, similar numbers of functional groups were observed for both reactions by XPS. Although these values differ slightly from those observed by TGA, as mentioned above, the carbon content considered in every technique is different and, in addition, XPS is a surface technique that is extrapolated to bulk materials, although the results obtained by XPS and TGA can be considered comparable.

Raman spectroscopy gives important information about the covalent modification of the carbon nanotubes. The spectrum for carbon nanotubes shows three zones of interest: the D band (1300–1400 $cm^{-1}$), which corresponds to the $sp^3$ carbon atoms; the G band (1500–1600 $cm^{-1}$), assigned to the $sp^2$ carbon atoms and the RBM (Radial Breathing Mode) region (150–350 $cm^{-1}$), which informs about the diameter and chirality of the nanotubes. In this case, bands between 180 and 240 $cm^{-1}$ are assigned to metallic nanotubes and bands between 250 and 310 $cm^{-1}$ to semiconducting nanotubes.[33] An increase in the ratio between the D and G bands is usually related to covalent functionalisation of the nanotubes, while modification of the RBM region can be used to analyse the kind of nanotubes (metallic or semiconducting) affected during functionalisation.[28,29] It should be noticed that only the SWCNTs with electronic structures in resonance or quasi-resonance with the excitation wavelength of the laser used for the analysis, *i.e.*, with specific chiralities and diameters, will be visible in the Raman spectra.[33,34] Therefore, a deep study of the reactivity of SWCNTs would require measurements at multiple wavelengths. Nonetheless, the predilection of the reactions for the attack to certain families of SWCNTs can be observed even using just one specific laser source.[35] For the matter of this study, a laser wavelength of 633 nm (Energy = 1.96 eV) was used. Figure 2 shows the Raman spectra of ***p*-SWCNTs**, **SWCNTs-1** and **SWCNTs-2**, with the inset showing a magnification of the D-Band. Additionally, Table 1 includes the ratios of the Raman D- to G-band areas ($I_D/I_G$). A higher value is observed in **SWCNTs-2** than in **SWCNTs-1**. The low intensity of the D band in carbon nanomaterials covalently modified by 1,3-dipolar cycloaddition of azomethine ylides has been observed previously in SWCNTs,[26] carbon nanohorns[36] and graphene[37] by some of us. Additionally, the RBM region of the Raman spectra has been analysed (Figure S3, Supporting Information). It can be seen that the

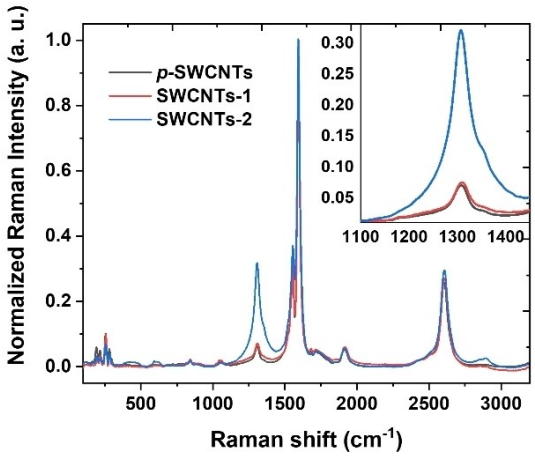


**Figure 2.** Normalized Raman spectra of ***p*-SWCNTs**, **SWCNTs-1** and **SWCNTs-2** using a laser source at 633 nm.

intensity of the bands between 250 and 310 $cm^{-1}$, associated with semiconducting nanotubes, only decreases for **SWCNTs-1**, remaining constant for **SWCNTs-2**. As such, it can be concluded that these kinds of carbon nanotubes are more affected by the Prato reaction. On the other hand, the bands between 180 and 240 $cm^{-1}$, associated with metallic nanotubes, are significantly reduced in **SWCNTs-1** and **SWCNTs-2**, thus meaning that the metallic nanotubes are affected by both reactions,[38] as already described by some authors. In addition, it is worth mentioning that the intensity of the bands associated with the metallic nanotubes does not decrease homogenously for the two reactions. This means that every reaction preferably attacks SWCNTs of some specific chiralities or diameters.[28] The work of Kataura is a very valuable tool for the assignment of the chirality of the tubes from the RBM region of the spectra of SWCNTs.[34] Figure S4 shows the RBM region of the Raman spectrum of the ***p*-SWCNTs** used in this work fitted with Voigtian functions. From this, six different SWCNTs were identified, (12,6); (12,3), (10,3), (9,4), (7,5) and (8,3). Table S1 summarizes the assigned chiralities and diameters as a function of the Raman shifts $\omega$. As it was already observed in Figure S3, SWCNTs at the lowest $\omega$, *i.e.*, metallic tubes with the lowest diameter, are the most reactive towards both reactions due to the pyramidalization of the carbon atoms within the SWCNT framework.[39] Within the smallest SWCNTs, both reactions seem to equally affect to those of chirality (12,3), while the tubes (12,6) are more affected by the Prato reaction (**SWCNTs-1**) than by the arylation (**SWCNTs-2**). The preferential functionalization of SWCNT specific chiralities by radical addition[38,40–43] and 1,3-dipolar cycloaddition[44,45] reactions has been already observed in multiple studies. Importantly, upshifts of the RBM frequencies can be observed in all the functionalized SWCNTs (Table S2). The extent of the movements correlates with the decreased in the intensity of the bands, *i.e.*, the spectra of the SWCNTs most affected by the reactions are more extensively modified. These movements are assigned to tube-tube interactions[46] and have been previously associated to the their debundled,[47,48] which is also induced with the functionalization.

The 1,3-dipolar cycloaddition and radical addition of diazonium salts were also carried out under classical conditions, *i.e.*, by conventional heating in solvents, to yield the derivatives **SWCNTs-3** and **SWCNTs-4**, respectively (Scheme S1, Supporting Information). TGA showed that the quantity of organic material introduced under these conditions is totally comparable to the quantity introduced under microwave irradiation (Figure S5, supporting information). However, when the Prato reaction is performed under classical conditions, the weight loss observed for **SWCNTs-3** starts at a lower temperature than for the tubes functionalised by microwave activation (**SWCNTs-1**). This can be attributed to annealing of the SWCNTs[49] as well as to the elimination of amorphous carbon[50] under microwave irradiation under solvent-free conditions. This behaviour has been described previously and is due to the strong adsorption of CNTs under these conditions, resulting in the generation of hot spots.[51] The high temperatures generated, which are not macroscopically measurable, can even produce holes in the glass vessels, which makes the use of quartz vessels necessary. When the Raman spectra are compared (Figure S6, supporting information), the $I_D/I_G$ values are similar for the derivatives obtained after radical addition (**SWCNTs-2** and **SWCNTs-4**), irrespective of the heating source, while the derivatives obtained after 1,3-dipolar cycloaddition display higher $I_D/I_G$ values when synthesized under conventional heating (**SWCNTs-3**) than under microwave irradiation (**SWCNTs-1**). As such, these observations agree with the TGA data. When the RBM region of the Raman spectra is analysed for the Prato reaction, the preferential modification of the metallic bands of SWCNTs (visible at 180–240 $cm^{-1}$ using a wavelength of 633 nm)[33] observed in the hybrids functionalised using microwave (**SWCNTs-1**) was not detected in the ones modified by classical heating (**SWCNTs-3**) (Figure S7a, Supporting Information). These data could be explained by the higher absorption of microwaves by metallic nanotubes when no solvent is used.[52] The analysis of the RBM region of SWCNTs modified by radical addition (Figure S7b, supporting information), shows that semiconducting SWCNTs are more affected in classical conditions (**SWCNTS-2**) than under microwave irradiation (**SWCNTs-4**). Metallic tubes are affected independently of the heating source, but certain selectivity between chiralities and diameters can be appreciated from the non-homogenous variation of the Raman band associated. As it was observed for SWCNTs functionalized under microwave irradiation, upshift of the RBM bands more decayed during the functionalization are also shown in the spectra of the samples modified by classical heating. In addition, a control experiment for the arylation reaction was carried out to shed light on the effects of the microwave irradiation. For this, ***p*-SWCNTs** were dispersed in water and heated in the microwave for 90 min (without reagents) and washed as **SWCNTs-2**. Figure S8 (a and b) shows the TGA and Raman spectra of the modified SWCNTs (**Control**) *vs* the ***p*-SWCNTs**. As expected, no appreciable alterations of the signatures of the tubes are observed after the microwave treatment as the solvent prevents the generation of the hot spots.

To study the performance of the reactions in greater detail, double functionalisation of ***p*-SWCNTs** was carried out under microwave conditions. Thus, **SWCNTs-2** previously modified by the diazonium salt reaction were subjected to the 1,3-dipolar cycloaddition reaction with sarcosine and 4-bromobenzaldehyde to yield **SWCNTs-5**, (Scheme 2). The bromine compound was chosen in order to be able to distinguish both functionalities by XPS.

Characterization of this derivative was also carried out using TGA and Raman spectroscopy, as well as XPS. Details of the analysis are shown in Table 2. As expected, the TGA shows an

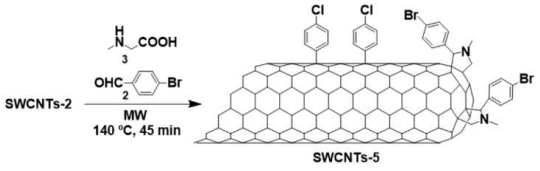


**Scheme 2.** Double functionalisation of ***p*-SWCNTs**: Prato reaction between 4-bromobenzaldehyde and sarcosine on **SWCNTs-2** using microwave activation.

**Table 2.** Details of the TGA, Raman and XPS analysis of **SWCNTs-5**.

| Sample | TGA | | | Raman | XPS[f] | | |
|---|---|---|---|---|---|---|---|
| | weight loss (%)[a] | C/FG[b] | | $I_D/I_G$[e] | C/Cl | C/Br | C/N |
| | | Tour[c] | Prato[d] | | | | |
| **SWCNTs-5** | 25 | 41 | 188 | 0.19 | 33 | 166 | 100 |

[a] Weight loss was measured by TGA at 700 °C, [b] Number of carbons per functional group: $C/F = [(100-\%_{weightloss})\times MW_{functionalgroup}]/12\times\%_{weightloss}$. Only the carbon atoms from the SWCNT walls are considered, and not the one introduced with the functional group. See section 2 in the Supporting Information for more information. [c] C/FG of the Tour reaction is taken from **SWCNTs-2** derivatives in Table 1. [d] The difference between the total weight loss and the weight loss after the first reaction (**SWCNTs-2** in Table 1) gives the C/F value of the Prato Reaction. [e] $I_D/I_G$ is the relative integrated area of the D band (*i.e.*, ranging from 1200 to 1400 $cm^{-1}$) and the G band (*i.e.*, ranging from 1400 to 1830 $cm^{-1}$) in the Raman spectra. [f] Carbon refers to the total number of carbon atoms in the sample, *i.e.*, those from the SWCNT walls and those introduced with the functional group.

increase in the weight loss from 17.9% in **SWCNTs-2** to 25% in **SWCNTs-5** (Figure S9a, Supporting Information). These results indicate that the Prato reaction introduced one functional group for every 186 carbon atoms, thus meaning that it proceeds to a much lesser extent in **SWCNTs-2** previously functionalised by radical addition than in ***p*-SWCNTs**. The Prato reaction is probably directed to more reactive sites on the sidewall of the carbon nanomaterials, which are presumably already filled by the arene groups.[26] XPS data indicate that one bromine functional group has been introduced every 166 carbon atoms in **SWCNTs-5** and, although slight differences can be appreciated, this nevertheless corroborates the TGA results. Chlorine is also present as it was previously introduced in **SWCNTs-2**. Different values are observed in XPS than in TGA as, in the former, carbon refers to the total carbon content. It should also be noted that the chlorine content varies as the total mass of the sample is different after double functionalisation. The Raman spectra of ***p*-SWCNTs**, **SWCNTs-2** and **SWCNTs-5** reveal that the area of the D-band decreases from **SWCNTs-2** to **SWCNTs-5** (Figure S9b, Supporting Information). This agrees with the previous results and indicates that the 1,3-dipolar cycloaddition carried out under solvent-free conditions and microwave irradiation reduces the number of defects in the carbon nanotubes.

Therefore, based on our results, we hypothesize that the Prato reaction does not create such a high number of defects (i.e., $sp^3$ carbon atoms) as the radical addition. This can be explained if the Prato reaction occurs at defects previously present in carbon nanomaterials while the more reactive radical reaction does not require the presence of such defects.

### *Calculations*

To shed more light on the differences between the two reactions, we performed DFT calculations to simulate the Raman spectra of pristine and functionalised single-walled carbon nanotubes using periodic boundary conditions. To this end, a defect-free zigzag (10,0) SWCNT was considered. As shown in Figure 3, the predicted Raman spectrum of the pristine ***p*-SWCNTs** exhibits a unique characteristic band ascribed to the G mode (see also Figure S10). In contrast, functionalisation in **SWCNTs-**1 (Figure S11) and **SWCNTs-2** (Figure S12) leads to the appearance of

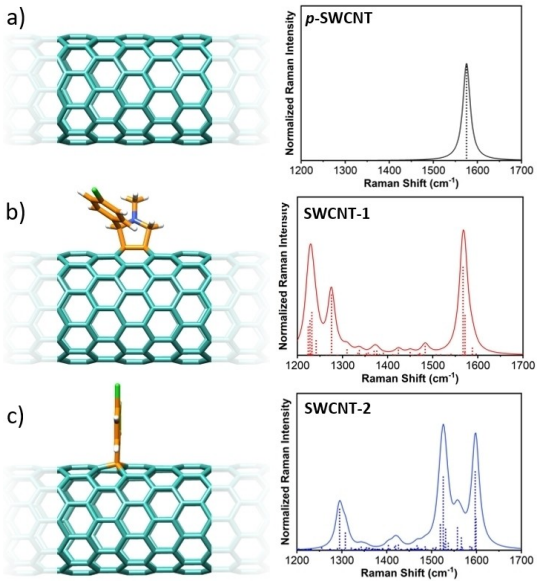


**Figure 3.** Optimized structures and Raman profiles of a) pristine, b) Prato- and c) Tour-functionalised (10,0) SWCNTs, with the dark-colored portion of the nanotubes indicating the unit cells. The Raman profiles for each nanotube are obtained by applying Lorentzian line broadening with a full width at half maximum of 20 $cm^{-1}$.

D modes due to the Raman scattering from a nonzero-center phonon mode emerging from the defects.[53,54] Interestingly, there are notable differences in the way the D and G modes are activated as a function of the different functionalisation. Thus, while Prato functionalisation activates the D modes to a greater extent, radical functionalisation preferentially activates the G modes. This effect can be explained in terms of the greater modification at the nanotube surface after Prato functionalisation because of the introduction of two $sp^3$-hybridized carbon lattice atoms into the regular $sp^2$ network. We calculated the $I_D/I_G$ intensity ratio by summing the Raman intensities in the D-region (*i.e.*, range from 1200 to 1400 $cm^{-1}$) and G-region (*i.e.*, range from 1400 to 1700 $cm^{-1}$), and found that Prato functionalisation gives a larger $I_D/I_G$ intensity ratio ($I_D/I_G = 1.37$) than Tour functionalisation ($I_D/I_G = 0.30$). Although the $I_D/I_G$ intensity ratio is commonly used as a measure of the degree of defect surface density,[38,54] our results shows that care must be taken when using this parameter to compare two different types of

functionalisations, such as those studied here, since the number of Raman-active D- and G-modes varies markedly in these two cases.

In order to analyse the role played by the different covalent functionalisations on defect-containing nanotubes, we now turn our attention to an analysis of the vibrational properties of nanotubes with defects. To this end, vacancy defects were introduced into the hexagonal structure of the carbon nanotubes. In particular, single- (SV) and double-vacancy (DV) defects were considered since they are the most common structural defects present in CNT sidewalls.[54–57] SVs originate from the removal of a single C atom from the hexagonal network, whereas DVs result from the removal of two C atoms, thus leading to the formation of two pentagons and one octagon ring (see Figure 4). In agreement with a previous study,[56] the loss of symmetry induced by these defects results in the activation of a large number of Raman modes (see Figure S13), which in turn results in an increased $I_D/I_G$ intensity ratio when compared to defect-free nanotubes (i.e., $I_D/I_G$ value of 0.28 and 0.49 for ***p*-SWCNT** with SV and DV defects, respectively).

We then studied the effects of different functionalisations on the Raman spectra for each type of defect (Figure S14). To this end, we functionalised the SV- and DV-containing nanotubes using the Prato and Tour approaches. Inspection of the Raman spectral profile for defect-containing **SWCNTs-2** shows that the G-mode splits into several bands with small intensities upon radical functionalisation (see Figure S15). However, this functionalisation with defect-containing nanotubes alters the relative intensities of the D- and G-bands only slightly when compared to defect-free **SWCNTs-2** (see Figure 4c). This reveals that radical addition gives very similar $I_D/I_G$ values in both defect-containing and defect-free nanotubes, thus corroborating the hypothesis that this type of functionalisation does not require the presence of defects.

Although Prato functionalisation splits the D-mode into several bands (Figure S16), the Raman spectral profile of defect-containing **SWCNTs-1** shows a reduction in the $I_D/I_G$ values of about 30% when compared to defect-free **SWCNTs-1**. Therefore, on the basis of the calculated data, we suggest that the Prato reaction, although is less reactive than the radical addition, can benefit from the defects previously present in carbon nanomaterials, which functionalises the nanotube without the appearance of a high number of defects.

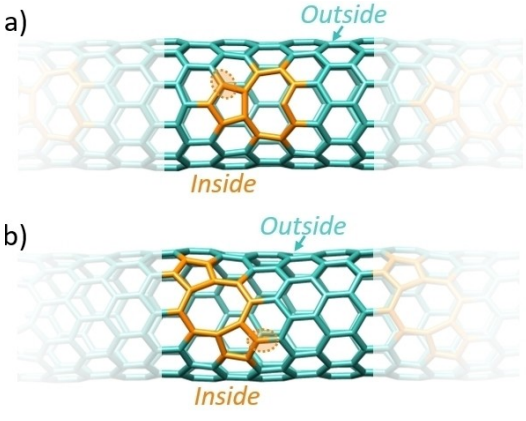


c)

| | Defect-free | SVs | DVs |
|---|---|---|---|
| **SWCNT-1** | 1.37 | 1.01 (0.72) | 1.05 (0.74) |
| **SWCNT-2** | 0.30 | 0.27 (0.27) | 0.21 (0.22) |

**Figure 4.** Optimized structures for a) SV and b) DV defects on the sidewall of ***p*-SWCNTs**, with the dark-colored portion of the nanotubes indicating the unit cells. The atoms involved in the defects are highlighted in orange. The position of inner and outer functionalisation is also illustrated. c) $I_D/I_G$ ratio of defect-free, and SV- and DV-containing **SWCNTs-1** and **SWCNTs-2** when functionalisation takes place inside the defects. The values shown in brackets correspond to nanotubes functionalised outside of the defects.

## Conclusions

Two different types of CNT functionalisation reactions have been analysed experimentally and theoretically herein. The number of groups introduced on the tubes using these reactions has been analysed using different characterisation techniques.

The results of this study support the idea that $I_D/I_G$ ratios obtained from Raman spectra are only useful for comparing functionalisations produced using the same type of reaction. As such, these values are of little use when comparing functionalisations produced using different reaction types.

Our observations also suggest that the Prato reaction could be more prone to attack positions close to defects on the tubes. When the reaction takes place under microwave irradiation, the number of $sp^3$ carbon atoms does not increase to the same extent as when functionalisation is performed using radical addition. Considering the importance of defect densities in the applications of carbon nanotubes, the Prato reaction could be preferred to obtain stable derivatives that preserve the electronic properties of SWCNTs.

## Experimental Section

### General Methods

Solvents and chemicals were purchased from Sigma-Aldrich (Madrid, Spain) and were used as received. Pristine SWCNTs were obtained from Carbon Nanotechnologies Inc. (HiPco® Single-Wall Carbon Nanotubes, lot number R0513) (See Section 1 in Supporting Information more information). Microwave irradiation was applied using a CEM Discover reactor with an infrared pyrometer, pressure control system, stirring and air-cooling option. The thermogravimetric analyses were performed with a TGA Q50 (TA Instruments) at 10 °C $min^{-1}$ under a $N_2$ atmosphere. Raman spectra were recorded with an Invia Renishaw microspectrometer equipped with an He–Ne laser at an excitation wavelength of 633 nm and a laser power of 0.17 mW (spectral resolution $< 1$ $cm^{-1}$).

X-ray photoelectron spectroscopy (XPS) analyses were performed using a VGMicrotech ESCA 3000Multilab, equipped with a dual Mg/Al anode. The spectra were excited by the unmonochromatized Al Kα source (1486.6 eV) run at 14 kV and 15 mA. The analyser was operated in constant analyser energy (CAE) mode. For the individual peak-energy regions, a pass energy of 20 eV set across the hemispheres was used. Survey spectra were measured at a pass energy of 50 eV.

The sample powders were analysed as pellets mounted on a double-sided adhesive tape. The pressure in the analysis chamber was in the range of $10^{-8}$ Torr during data collection. Constant charging of the samples was removed by referencing all energies to the C 1s set at 284.4 eV, on the main C 1s peak of SWCNTs. The invariance of the peak shapes and widths at the beginning and end of the analyses ensured the absence of differential charging. Peak analyses were performed with the software provided by VG, based on a non-linear least squares fitting program using a weighted sum of Lorentzian and Gaussian component curves after background subtraction according to Shirley and Sherwood.[58,59] XPS atomic ratio were obtained by the ratio of C1s/Cl2p3/2, C1s/Br3d5 and C1s/N1s intensity peaks normalized by the sensitivity factor provided by the analysis software. The binding energy values are quoted with a precision of $\pm 0.15$ eV and the atomic percentage with a precision of $\pm 10\%$.

### Synthesis of SWCNTs-1 and SWCNTs-5: Prato reaction.

10 mg of ***p*-SWCNTs** or **SWCNTs-2** was suspended in $CH_2Cl_2$ (5 mL) with 0.264 mmol of 4-chlorobenzaldehyde **1** (37.1 mg) or 4-bromobenzaldehyde **2** (48.8 mg) and sarcosine **3** (23.5 mg, 0.264 mmol) in a microwave quartz vessel. After sonication for 5 min, the solvent was evaporated under a nitrogen stream. The vessel was subsequently closed and introduced into a monomode microwave, where the mixture was irradiated for 45 minutes at different powers and temperatures.[26] After that time, the crude reaction mixture was resuspended in 25 mL of $CH_2Cl_2$ and sonicated for 5 min. The solution was filtered through a Millipore membrane (PTFE, 0.2 μm), and the black solid collected was washed with 75 mL of methanol and 75 mL of $CH_2Cl_2$ (sonicated and filtered), then dried under high vacuum to afford **SWCNTs-1** or **SWCNTs-5**.

### Synthesis of SWCNTs-2: Radical addition

10 mg of ***p*-SWCNTs** was sonicated in deionized water (20 mL) together with 4-chloroaniline **4** (220.6 mg, 1.73 mmol) for 10 min in a microwave glass vessel. Finally, isoamyl nitrite **5** (0.11 mL, 0.835 mmol) was added, and a condenser was inserted. The mixture was irradiated at 80 °C with a monomode microwave working at 100 W for 30 min and, after addition of a new aliquot of isoamyl nitrite **5** (0.11 mL, 0.835 mmol), at 30 W for 60 min. After cooling to room temperature, the crude reaction mixture was filtered through a Millipore membrane (GTTP, 0.2 μm). The black solid collected was washed using cycles of sonication and filtration with methanol until the filtrate was clear, then dried under high vacuum to afford **SWCNTs-2.**

### DFT Calculations: Computational Method

As a first step, single infinite one-dimensional chains (1D) were constructed from a molecular fragment of zigzag (10,0) nanotube comprising 120 carbon atoms built using the CaGe package,[60] applying a lattice vector of 12.674 Å along the *x*-axis. Prato and Tour functionalisation was performed to build **SWCNTs-1** and **SWCNTs-2**, thus leading to unit cells comprising 141 and 131 atoms, respectively. For the defect-containing nanotubes, single- (SVs) and double-atom vacancies (DVs) were generated by removing one and two C atoms from the hexagonal network of the sidewall, respectively.

Once the systems had been built, full geometry optimizations (simultaneous lattice/cell and structure optimizations) in the framework of periodic boundary conditions (PBCs) were performed using the density functional theory (DFT) approach as implemented in the CRYSTAL17 software package.[61,62] The hybrid generalized gradient approximation (GGA) functional PBE0[63] together with the 6-31G** basis set,[64,65] as well as Grimme DFT-D3 semiempirical dispersion to take into account vdW corrections,[66] were used for the geometry optimizations. All atoms were allowed to vary independently with no constraints. Reciprocal space sampling was performed using a shrinking factor of 4 4, a tolerance for Coulomb and exchange integral cutoffs (TOLINTEG parameter) of 7 7 7 7 18, and a tolerance on the change of total energies (TOLDEE parameter) of 8 ($\Delta E < 10^{-8}$ Hartree).

In a subsequent step, the Raman intensities of the previously optimized 1D chains were calculated using the hybrid generalized gradient approximation (GGA) functional PBE0 and the 6-21G* basis set.[67,68] In this case, a TOLDEE value of 10 ($\Delta E < 10^{-10}$ hartree) was used. Eigenvalues and eigenvectors were calculated numerically using the harmonic approximation[69] and Raman intensities were calculated using the CPHF analytical approach.[69,70] The Raman profiles for each nanotube were obtained by applying Lorentzian line broadening with a full width at half-maximum of 20 $cm^{-1}$, with the frequencies being scaled down by a factor of 0.961 to disentangle experimental misassignments.

## Supporting Information

The authors have cited additional references within the Supporting Information.[71]

## *Acknowledgements*

The authors acknowledge financial support from the Spanish government (project PID2020-113080RB-I00) and the Junta de Comunidades de Castilla-La Mancha (project SBPLY/21/180501/000135/1). This study forms part of the Advanced Materials program and was supported by MCIN with funding from European Union NextGenerationEU (PRTR-C17.I1) and by the Junta de Comunidades de Castilla-La Mancha. The work at the University of Málaga was funded by the MICINN (PID202-139548NB-I00) and by the Junta de Andalucía (P18-FR-4559) projects. The authors thankfully acknowledge the computer resources, technical expertise, and assistance provided by the SCBI (Supercomputing and Bioinformatics) centre of the University of Málaga. M. I. L. acknowledges her Juan de la Cierva Incorporación grant (IJC 2018-035355-I) funded by MCIN/AEI/10.13039/501100011033. Funded with Aid for First Research Projects (PAID-06-22), Vice-rectorate for Research of the Universitat Politècnica de València (UPV).

## *Conflict of Interests*

The authors declare no conflict of interest.

## *Data Availability Statement*

The data that support the findings of this study are available from the corresponding author upon reasonable request.

**Keywords:** DFT calculations · organic functionalisation · Prato reaction · Raman spectroscopy · single-walled carbon nanotubes

[1] S. Iijima, *Nature* **1991**, *354*, 56–58.
[2] A. V. V. V. Ravi Kiran, G. Kusuma Kumari, P. T. Krishnamurthy, *J. Drug Delivery Sci. Technol.* **2020**, *59*, 101892.
[3] G. Hong, S. Diao, A. L. Antaris, H. Dai, *Chem. Rev.* **2015**, *115*, 10816–10906.
[4] V. Campisciano, M. Gruttadauria, F. Giacalone, *ChemCatChem* **2019**, *11*, 90–133.
[5] I. A. Kinloch, J. Suhr, J. Lou, R. J. Young, P. M. Ajayan, *Science.* **2018**, *362*, 547–553.
[6] L. Wieland, H. Li, C. Rust, J. Chen, B. S. Flavel, *Adv. Energy Mater.* **2021**, *11*, 2002880.
[7] X. Liu, Y. Ying, J. Ping, *Biosens. Bioelectron.* **2020**, *167*, 112495.
[8] J. Ackermann, J. T. Metternich, S. Herbertz, S. Kruss, *Angew. Chem. Int. Ed.* **2022**, *61*, e202112372.
[9] L. Qian, Y. Xie, M. Zou, J. Zhang, *J. Am. Chem. Soc.* **2021**, *143*, 18805–18819.
[10] H. Ali-Boucetta, A. Nunes, R. Sainz, M. A. Herrero, B. Tian, M. Prato, A. Bianco, K. Kostarelos, *Angew. Chem. Int. Ed.* **2013**, *52*, 2274–2278.
[11] Z. Syrgiannis, M. Melchionna, M. Prato, in *Encycl. Polym. Nanomater.*, **2016**, pp. 1–8.
[12] D. Tasis, N. Tagmatarchis, A. Bianco, M. Prato, *Chem. Rev.* **2006**, *106*, 1105–1136.
[13] Z. Syrgiannis, V. La Parola, C. Hadad, M. I. M. Lucío, E. Vázquez, F. Giacalone, M. Prato, *Angew. Chem. Int. Ed. Engl.* **2013**, *52*, 1–5.
[14] Z. Syrgiannis, A. Bonasera, E. Tenori, V. La Parola, C. Hadad, M. Gruttadauria, F. Giacalone, M. Prato, *Nanoscale* **2015**, *7*, 6007–6013.
[15] R. Dubey, D. Dutta, A. Sarkar, P. Chattopadhyay, *Nanoscale Adv.* **2021**, *3*, 5722–5744.
[16] M. Matiyani, M. Pathak, B. S. Bohra, N. G. Sahoo, *Handb. Carbon Nanotub.* **2022**, *42*, 421–448.
[17] B. Dinesh, A. Bianco, C. Ménard-Moyon, *Nanoscale* **2016**, *8*, 18596–18611.
[18] V. Georgakilas, K. Kordatos, M. Prato, D. M. Guldi, M. Holzinger, A. Hirsch, *J. Am. Chem. Soc.* **2002**, *124*, 760–761.
[19] J. L. Bahr, J. M. Tour, *Chem. Mater.* **2001**, *13*, 3823–3824.
[20] S. Aroua, Y. Yamakoshi, *J. Am. Chem. Soc.* **2012**, *134*, 20242–20245.
[21] S. Iftikhar, S. Aslam, N. Z. Butt, R. S. Ashraf, B. Yameen, *J. Mater. Chem. C* **2020**, *8*, 17365–17373.
[22] D. Lang, A. Krueger, *Diamond Relat. Mater.* **2011**, *20*, 101–104.
[23] S. Alidori, D. L. J. Thorek, B. J. Beattie, D. Ulmert, B. A. Almeida, S. Monette, D. A. Scheinberg, M. R. McDevitt, *PLoS One* **2017**, *12*, 1–25.
[24] Y. Zhao, T. Zhao, Y. Cao, J. Sun, Q. Zhou, H. Chen, S. Guo, Y. Wang, Y. Zhen, X. J. Liang, et al., *ACS Nano* **2021**, *15*, 6517–6529.
[25] P. Oskin, I. Demkina, E. Dmitrieva, S. Alferov, *Nanomaterials* **2023**, *13*, 1–21.
[26] F. G. Brunetti, M. A. Herrero, J. D. M. Muñoz, A. Díaz-Ortiz, J. Alfonsi, M. Meneghetti, M. Prato, E. Vázquez, *J. Am. Chem. Soc.* **2008**, *130*, 8094–8100.
[27] M. I. Lucío, R. Opri, M. Pinto, A. Scarsi, J. L. G. Fierro, M. Meneghetti, G. Fracasso, M. Prato, E. Vázquez, M. A. Herrero, *J. Mater. Chem. B* **2017**, *5*, 8821–8832.
[28] R. Graupner, *J. Raman Spectrosc.* **2007**, *38*, 1538–1553.
[29] C. A. Dyke, J. M. Tour, *J. Phys. Chem. A* **2004**, *108*, 11151–11159.
[30] A. Setaro, M. Adeli, M. Glaeske, D. Przyrembel, T. Bisswanger, G. Gordeev, F. Maschietto, A. Faghani, B. Paulus, M. Weinelt, et al., *Nat. Commun.* **2017**, *8*, 1–7.
[31] G. Bottari, M. Ángeles Herranz, L. Wibmer, M. Volland, L. Rodríguez-Pérez, D. M. Guldi, A. Hirsch, N. Martín, F. D'Souza, T. Torres, *Chem. Soc. Rev.* **2017**, *46*, 4464–4500.
[32] J. F. Moulder, W. F. Stickle, P. E. Sobol, K. D. Bomben, *Handbook of X-Ray Photoelectron Spectroscopy*, Physical Electronics Division (Perkin-Elmer Corporation), Minnesota, **1992**.
[33] J. Maultzsch, H. Telg, S. Reich, C. Thomsen, *Phys. Rev. B: Condens. Matter Mater. Phys.* **2005**, *72*, 205438.
[34] H. Kataura, Y. Kumazawa, Y. Maniwa, I. Umezu, S. Suzuki, Y. Ohtsuka, Y. Achiba, *Synth. Met.* **1999**, *103*, 2555–2558.
[35] E. Menna, F. Della Negra, M. Dalla Fontana, M. Meneghetti, *Phys. Rev. B: Condens. Matter Mater. Phys.* **2003**, *68*, 193412.
[36] N. Rubio, M. A. Herrero, M. Meneghetti, Á. Díaz-Ortiz, M. Schiavon, M. Prato, E. Vázquez, *J. Mater. Chem.* **2009**, *19*, 4407.
[37] M. Quintana, K. Spyrou, M. Grzelczak, W. R. Browne, P. Rudolf, M. Prato, *ACS Nano* **2010**, *4*, 3527–3533.
[38] M. Schirowski, C. Tyborski, J. Maultzsch, F. Hauke, A. Hirsch, J. Goclon, *Chem. Sci.* **2019**, *10*, 706–717.
[39] Z. Chen, W. Thiel, A. Hirsch, *ChemPhysChem* **2003**, *4*, 93–97.
[40] W. J. Kim, M. L. Usrey, M. S. Strano, *Chem. Mater.* **2007**, *19*, 1571–1576.
[41] M. S. Strano, C. A. Dyke, M. L. Usrey, P. W. Barone, M. J. Allen, H. Shan, C. Kittrell, R. H. Hauge, J. M. Tour, R. E. Smalley, *Science.* **2003**, *301*, 1519–1522.
[42] L. R. Powell, M. Kim, Y. Wang, *J. Am. Chem. Soc.* **2017**, *139*, 12533–12540.
[43] M. S. Strano, *J. Am. Chem. Soc.* **2003**, *125*, 16148–16153.
[44] M. Bayazit, K. Coleman, *J. Am. Chem. Soc.* **2009**, *131*, 10670–10676.
[45] X. Lu, F. Tian, X. Xu, N. Wang, Q. Zhang, *J. Am. Chem. Soc.* **2003**, *125*, 10459–10464.
[46] M. S. Dresselhaus, G. Dresselhaus, R. Saito, A. Jorio, *Phys. Rep.* **2005**, *409*, 47–99.
[47] A. M. Díez-Pascual, M. Naffakh, J. M. González-Domínguez, A. Ansón, Y. Martínez-Rubi, M. T. Martínez, B. Simard, M. A. Gómez, *Carbon* **2010**, *48*, 3485–3499.
[48] S. Utsumi, M. Kanamaru, H. Honda, H. Kanoh, H. Tanaka, T. Ohkubo, H. Sakai, M. Abe, K. Kaneko, *J. Colloid Interface Sci.* **2007**, *308*, 276–284.
[49] W. Lin, K. Moon, S. Zhang, Y. Ding, J. Shang, M. Chen, C. Wong, *ACS Nano* **2010**, *4*, 1716–1722.
[50] E. Vázquez, V. Georgakilas, M. Prato, *Chem. Commun.* **2002**, *2*, 2308–2309.
[51] T. J. Imholt, C. A. Dyke, B. Hasslacher, J. M. Perez, D. W. Price, J. A. Roberts, J. B. Scott, A. Wadhawan, Z. Ye, J. M. Tour, *Chem. Mater.* **2003**, *15*, 3969–3970.
[52] B. R. Priya, H. J. Byrne, *J. Phys. Chem. C* **2009**, *113*, 7134–7138.
[53] A. C. Ferrari, J. Robertson, *Phys. Rev. B: Condens. Matter Mater. Phys.* **2000**, *61*, 14095.
[54] G. Giambastiani, S. Cicchi, A. Giannasi, L. Luconi, A. Rossin, F. Mercuri, C. Bianchini, A. Brandi, M. Melucci, G. Ghini, et al., *Chem. Mater.* **2011**, *23*, 1923–1938.
[55] P. Vinten, P. Marshall, J. Lefebvre, P. Finnie, *J. Phys. Chem. C* **2013**, *117*, 3527–3536.
[56] W. A. Saidi, *J. Phys. Chem. A* **2014**, *118*, 7235–7241.
[57] R. B. Hudson, A. Sinha, *Carbon* **2018**, *138*, 81–89.
[58] D. A. Shirley, *Phys. Rev. B* **1972**, *5*, 4709–4714.
[59] P. M. A. Sherwood, *Practical Surface Analysis*, Wiley-VCH Verlag, New York, **1990**.
[60] G. Brinkmann, O. D. Friedrichs, S. Lisken, A. Peeters, N. Van Cleemput, *MATCH Commun. Math. Comput. Chem.* **2010**, *63*, 533–552.
[61] A. Erba, J. Baima, I. Bush, R. Orlando, R. Dovesi, *J. Chem. Theory Comput.* **2017**, *13*, 5019–5027.
[62] R. Dovesi, A. Erba, R. Orlando, C. M. Zicovich-Wilson, B. Civalleri, L. Maschio, M. Rérat, S. Casassa, J. Baima, S. Salustro, et al., *Wiley Interdiscip. Rev.: Comput. Mol. Sci.* **2018**, *8*, e1360.
[63] J. P. Perdew, M. Ernzerhof, K. Burke, *J. Chem. Phys.* **1996**, *105*, 9982–9985.
[64] M. M. Francl, W. J. Pietro, W. J. Hehre, J. S. Binkley, M. S. Gordon, D. J. DeFrees, J. A. Pople, *J. Chem. Phys.* **1982**, *77*, 3654–3665.
[65] W. J. Hehre, K. Ditchfield, J. A. Pople, *J. Chem. Phys.* **1972**, *56*, 2257–2261.
[66] J. Antony, S. Ehrlich, H. J. Krieg, *J. Chem. Phys.* **2010**, *132*, 154104..
[67] H. Su, G. Ma, Y. Liu, *Theor. Chim. Acta* **1973**, *28*, 213–222.
[68] J. S. Binkley, J. A. Pople, W. J. Hehre, *J. Am. Chem. Soc.* **1980**, *102*, 939–947.
[69] F. Pascale, C. M. Zicovich-Wilson, F. López-Gejo, B. Civalleri, R. Orlando, R. Dovesi, *J. Comput. Chem.* **2004**, *25*, 888–897.
[70] C. M. Zicovich-Wilson, F. Pascale, C. Roetti, V. R. Saunders, R. Orlando, R. Dovesi, *J. Comput. Chem.* **2004**, *25*, 1873–1881.
[71] N. Rubio, M. A. Herrero, A. de la Hoz, M. Meneghetti, M. Prato, E. Vázquez, *Org. Biomol. Chem.* **2010**, *8*, 1936–1942.

Manuscript received: July 31, 2023
Accepted manuscript online: October 3, 2023
Version of record online: November 6, 2023